ELSEVIER

Contents lists available at ScienceDirect

Extreme Mechanics Letters

journal homepage: www.elsevier.com/locate/eml



Non-reciprocal flexural wave propagation in a modulated metabeam



H. Nassar^a, H. Chen^a, A.N. Norris^b, G.L. Huang^{a,*}

- ^a Department of Mechanical and Aerospace Engineering, University of Missouri, Columbia, MO 65211, USA
- ^b Department of Mechanical and Aerospace Engineering, Rutgers University, Piscataway, NJ 08854-8058, USA

ARTICLE INFO

Article history: Received 30 April 2017 Received in revised form 3 July 2017 Accepted 3 July 2017 Available online 14 July 2017

Keywords: Non-reciprocity directional bandgap one-way mode conversion coupled mode theory

ABSTRACT

Flexural wave propagation in an Euler–Bernoulli beam coupled to a set of spring–mass resonators is investigated in the presence of a pump wave in the form of a space–time modulation of the beam-resonators coupling stiffness. A phase matching condition implies then that waves incident along or against the pump wave behave differently and gives rise in select frequency bands to one-way blocking and conversion of waves. In particular, one-way optical–acoustic transitions are proven possible and are quantified. Various orders of magnitude of relevant physical quantities, such as gap widths and interaction lengths, are estimated so as to guide future experimental implementations.

© 2017 Elsevier Ltd. All rights reserved.

1. Introduction

Dynamic materials or spatio-temporal composites are materials whose properties change not only in space but also with time. Unlike smart structures that can adapt to slowly changing environments and loadings, the constitutive properties of dynamic materials vary at a rate comparable to the frequency of waves traveling through. In doing so, dynamic materials become a playground for completely new wave phenomena [1–3]. Recently, in the context of breaking time-reversal symmetry and reciprocity in linear non-lossy elastic media, a particular class of dynamic materials with properties modulated in space and in time in a periodic wave-like fashion have allowed to achieve new functionalities in selective and directional wave control including reversed Doppler effect [4,5], one-way mode conversion [6–8], unidirectional bandgaps [9,10] and broadband quasistatic unidirectional wave acceleration [1,11].

There is a variety of ways in which space–time wave-like modulations, so-called "pump waves", can be generated. Most require the mechanical system to be active or to be coupled to some active components. For instance, the elastic stiffness can be wave-like modulated by shedding a moving train of laser beams on a photoelastic medium [9,12] or by controlling the electric input of a stack of piezoelectric components [13–15]. Further, both mass density and bulk modulus can be controlled by appropriately distributing a magnetic field over a magnetorheological elastomer [16]. The pump wave can also be of a mechanical origin by following a

"small-on-large" approach. In this scheme, a large-amplitude disturbance playing the role of a pump wave will effectively change the properties of the host medium by a non-linear mechanism (e.g., shock waves [4,5], or contact [17,18]) for any small-amplitude disturbance playing the role of the traveling wave.

In this letter, we investigate flexural wave propagation in a modulated metabeam (Fig. 1). In particular, we demonstrate, using asymptotic and numerical methods, a number of non-reciprocal effects including one-way conversion and blocking of waves. The use of a metabeam as a benchmark for these phenomena has a threefold motivation. First, a metabeam has a dispersive behavior accentuated by the resonance phenomenon. The resulting enriched dispersion diagram allows, under the influence of a pump wave, to observe several non-reciprocal effects simultaneously, a possibility that is precluded in the absence of dispersion and/or of optical branches [9,10]. Second, in the suggested benchmark, the beamresonators coupling stiffness is more accessible for modulation in an experimental setting than what has been suggested elsewhere [7] as evidenced by the work of Casadei et al. [13] and Chen et al. [14,15]. Third, the use of resonators allows to bring to low frequencies scattering phenomena otherwise only observable at phononic frequencies and further permits to control the onset frequency of these phenomena in a way that is unaffected by geometrical parameters.

2. Theory

We begin by coupling the motion u(x, t) of an Euler–Bernoulli beam with the motion v(x, t) of a set of resonators as illustrated on Fig. 1 so that the governing equations read

$$G\partial_x^4 u + \rho \partial_t^2 u = \frac{1}{d} \widetilde{h}(v - u), \qquad m\partial_t^2 v = \widetilde{h}(u - v),$$
 (1)

^{*} Corresponding author.

E-mail address: huangg@missouri.edu (G.L. Huang).

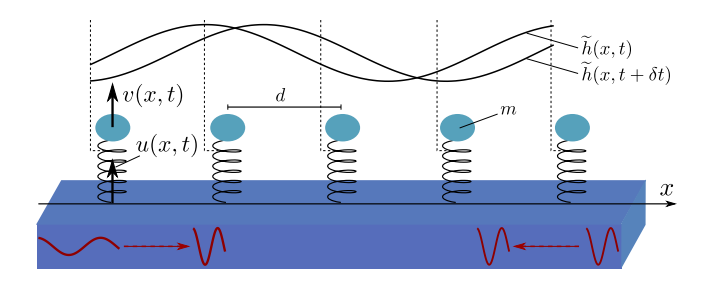


Fig. 1. Schematic of wave propagation in a modulated metabeam.

where G and ρ respectively are bending stiffness and mass density per unit length of the beam, m is the mass of a resonator, h is the modulated spring constant coupling the resonators to the beam and d is the spacing between two consecutive resonators. Although originally defined over a discrete set of locations where resonators are attached, h is assumed to be a function of the continuous variable x, which is a valid hypothesis in the long wavelength regime of interest in this letter. For later use, we introduce mass density per unit length of the resonators $\rho' = m/d$ and the normalized spring constant h is h in h i

The modulation is assumed weak in the sense that the perturbation δk is small compared to the uniform offset k. Weak modulations are of interest as they offer control over unidirectional scattering and conversion phenomena in a way that is unmatched in strongly modulated media. The fact that the considered modulation is sinusoidal is of lesser importance and will not play a significant role in what follows. Weak sine-wave-like modulations of non-dispersive media have been studied in earlier works in the context of parametric amplification by many authors [19–23]. Here, we build on their work and extend their results to this case study where strong dispersion effects and multiple dispersion branches are at play.

In the absence of the modulation, a harmonic plane wave $u_0(x,t)=U_0e^{i(q_0x-\omega_0t)}$ will propagate through the beam if it satisfies the dispersion relation $D(q_0,\omega_0)=0$ with

$$D(q, \omega) = Gq^4 - \rho_{\text{eff}}(\omega)\omega^2, \qquad \rho_{\text{eff}}(\omega) = \rho + \frac{m/d}{1 - \omega^2/\Omega^2},$$
 (2)

where $\Omega=\sqrt{h/m}$ is the resonance frequency of the resonators. In the presence of the modulation, the incident wave u_0 will be scattered thus generating a second wave $u_j(x,t)=U_je^{i(q_jx-\omega_jt)}$ whose wavenumber and frequency satisfy $D(q_j,\omega_j)=0$ and are given thanks to Floquet–Bloch theorem by the phase matching condition

$$q_j = q_0 + jq_m, \qquad \omega_j = \omega_0 + j\omega_m, \tag{3}$$

where j is a non-zero integer. Waves u_0 and u_j are thus seen as two modes traveling in the non-modulated metabeam but coupled by the modulation: when one is incident, the other is scattered. Consequently, scattered modes are solutions to the equations $D(q_0, \omega_0) = D(q_j, \omega_j) = 0$, or thanks to the phase matching condition, $D(q_0, \omega_0) = D(q_0 + jq_m, \omega_0 + j\omega_m) = 0$. These solution modes can be determined graphically; see Fig. 2. Other non-solution modes are not coupled: when one is incident, no scattered wave is generated, at least in the context of the present leading order theory [24].

At this stage, the directional behavior of the metabeam can be anticipated. As a matter of fact, from Fig. 2, it is seen that when two modes (q_0, ω_0) and (q_j, ω_j) are coupled, modes $(-q_0, \omega_0)$ and $(-q_j, \omega_j)$ are not. Thus, a wave form scattered if incident to the left will not be scattered if incident to the right and vice versa.

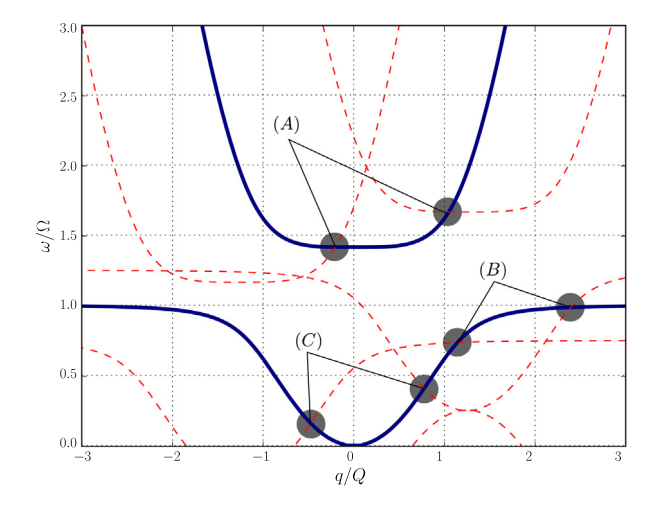


Fig. 2. The dispersion curve of the non-modulated metabeam (solid line) translated by $\pm(q_m,\omega_m)$ (dashed lines). The parameters of the modulation are $q_m=1.25Q$ and $\omega_m=0.25~\Omega$. Pairs of intersection points labeled A, B and C correspond to pairs of coupled modes: when one is incident, the other is scattered. Here, the first legs of pairs A, B and C are given by $\omega_0^A=1.41\Omega$, $q_0^A=-0.2Q$, $\omega_0^B=0.73~\Omega$, $q_0^B=1.14Q$, $\omega_0^C=0.15~\Omega$ and $q_0^C=-0.48Q$ whereas the second ones are obtained by translation: $\omega_1^{A,B,C}=\omega_0^{A,B,C}+\omega_m$ and $q_1^{A,B,C}=q_0^{A,B,C}+q_m$.

When it occurs, scattering will modify the wavenumbers and frequencies of the traveling waves so that the state of the modulated beam to leading order becomes

$$u(x,t) = \left(U_0 e^{i(q_0 x - \omega_0 t)} + U_i e^{i(q_j x - \omega_j t)}\right) e^{i(\delta q x - \delta \omega t)} \tag{4}$$

where δq and $\delta \omega$ are first order corrections to $q_{0,j}$ and $\omega_{0,j}$. Their inverses $1/\delta q$ and $1/\delta \omega$ will define the characteristic space and time scales of the interaction between incident and scattered waves. In particular, $1/\delta q$ will be interpreted as the penetration depth of a blocked wave or the conversion distance of a transmitted wave (see Eqs. (7) and (9) below). Inserting this ansatz into the governing equations, we recover a couple of compatibility equations reading

$$\begin{bmatrix} 4q_0^3G\Pi(\delta q - \delta\omega/c_0) & \rho'^2\omega_0^2\omega_j^2\overline{\delta_jk} \\ \rho'^2\omega_0^2\omega_j^2\delta_jk & 4q_j^3G\Pi(\delta q - \delta\omega/c_j) \end{bmatrix} \begin{bmatrix} U_0 \\ U_j \end{bmatrix} = \begin{bmatrix} 0 \\ 0 \end{bmatrix}$$
(5)

where $\delta_j k$ is the jth Fourier component of the modulation, $\Pi = (k - \rho' \omega_0^2)(k - \rho' \omega_j^2)$ and $c_{0,j}$ is group velocity $-\partial D/\partial q/\partial D/\partial \omega(q_{0,j}, \omega_{0,j})$.

3. Results

In our context, that of a modulation with a unique Fourier component, it is enough to consider $i = \pm 1$ since otherwise $\delta_i k$ vanishes but the results generalize immediately to modulations with multiple Fourier components. By setting the determinant of the above system to zero, the corrections $(\delta q, \delta \omega)$ can be determined for each pair of coupled modes $(q_{0,j}, \omega_{0,j})$; see Fig. 3(I-a,b). The resulting dispersion curve is shown on Fig. 3(II). Finite difference techniques were used to simulate a few broadband transient responses of the modulated metabeam Appendix C. The spectral content of these responses was obtained using discrete Fourier transform in space and in time and then used to numerically approximate the dispersion curve. Both numerical and asymptotic approximations match closely as shown on Fig. 3(II). Unless otherwise specified, illustrated results are obtained with the parameters $\rho/\rho'=1$, $q_m=1.25Q$, $\omega_m=0.25~\Omega$ and $\delta k/k=0.1$ with $Q = \sqrt[4]{k/G}$.

The dispersion curve reveals the existence of a couple of directional bandgaps whereby waves are blocked over a frequency

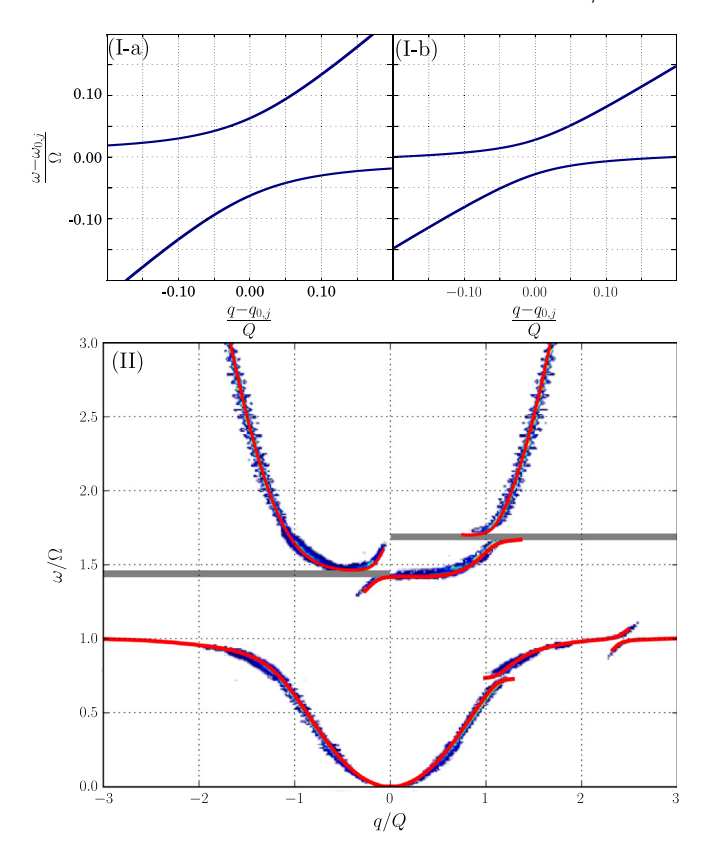


Fig. 3. First order corrections to the dispersion curve of a modulated metabeam in the vicinity of pair A (I-a) and B (I-b). Corrections in the vicinity of pair C are negligible and omitted. The overall resulting dispersion curve (red solid lines) is depicted on (II) and appears to match its numerically obtained counterpart (level set). A couple of narrow directional bandgaps is highlighted. (For interpretation of the references to color in this figure legend, the reader is referred to the web version of this article.)

range if incident in a given direction but are transmitted if incident in the opposite direction. More generally, as a result to the asymmetric nature of the phase matching condition, parity of the dispersion curve is lost, a symptom of the breaking of time-reversal symmetry and reciprocity. Quantitatively, pairs of coupled modes will open a pair of directional gaps whenever $q_0q_j < 0$ in which case the gaps will extend over the band $\omega_0 + \delta \omega$ on one side of the dispersion diagram, and over the band $\omega_j + \delta \omega$ on the opposite side, with (see Appendix A)

$$0 \le |\delta\omega| < \frac{\rho'^2 \omega_0^2 \omega_j^2 |\delta_j k|}{2G |(q_0 q_j)^{3/2} \Pi|} \frac{1}{|1/c_0 - 1/c_j|} \equiv \delta\omega_{\text{max}}.$$
 (6)

The penetration depth of an incident wave of frequency $\omega_0 + \delta \omega$ falling within the gap is of the order of the inverse of the imaginary part of $\delta q \equiv \delta q(\delta \omega)$, namely,

$$\Im(\delta q) = \frac{\left|1/c_0 - 1/c_j\right|}{2} \sqrt{\delta \omega_{\text{max}}^2 - \delta \omega^2}.$$
 (7)

Beyond this depth, the incident wave is completely reflected and transformed into a wave of frequency $\omega_i + \delta \omega$.

Having a fixed geometry, the modulation parameters q_m and ω_m can be tuned in order to maximize the width of the bandgap $\delta\omega_{\rm max}$ as well as the associated decay speed $\Im(\delta q)$. Fig. 4 shows how these two objective functions vary with respect to the output frequency ω_j for a given input mode (q_0,ω_0) . Various observations on how these quantities compete can be made. For instance, maximum decay speed is achieved at the boundaries of the main gap (shaded area) but then the newly opened gap would be of infinitesimal

width as $\delta\omega_{\rm max}$ approaches zero. Further, maximum gap width is obtained for $\omega_j=\omega_0$; however, in that case, $\omega_m=0$ and the gap is bidirectional. Therefore, the best compromise appears to be realized at the non-global local maximum of $2\omega_{\rm max}/\Omega$, around $\omega_j/\Omega\approx0.8$. Note that in this case, the reflected mode is an acoustic mode $(\omega_j<\Omega)$ whereas the incident mode is an optical one $(\omega_0>\Omega)$. This is one example of one-way optical-acoustic conversion by reflection, another example of one-way optical-acoustic conversion but in transmission is detailed later on. Fig. 4 also clarifies why pair C features negligible scattering effects compared to pairs A and B (Fig. 3). Pair C lies in fact in a low frequency band away from the resonance where both the directional gap width and decay speed approach zero.

Besides one-way blocking of waves, the modulated metabeam features one-way conversion/transmission phenomena when $q_0q_j>0$. Suppose that a wave of frequency $\omega_0+\delta\omega$ traveling inside a non-modulated metabeam penetrates at x=0 into a modulated region. Call $\delta q_\pm = \delta q_s \pm \delta q_d$ the two roots of the dispersion relation $\delta q = \delta q(\delta\omega)$ and $C_\pm = U_j/U_0$ the corresponding coupling strengths, then the real total field reads

$$u(x \ge 0, t) = \Re \left\{ A e^{i(\delta q_s x - \delta \omega t)} \left\{ (C_- - C_+) \cos(\delta q_d x) u_0(x, t) + i \sin(\delta q_d x) [(C_+ + C_-) u_0(x, t) + 2 u_i(x, t)] \right\} \right\}, \quad (8)$$

where A is an arbitrary complex amplitude and u_0 and u_1 are taken to be of unitary amplitudes (see Appendix B). Therefore, mode u_0 has a decreasing amplitude and reaches its minimum at $x=\pi/(2\delta q_d)$ while, simultaneously, the mixed mode $(C_++C_-)u_0/2+u_j$ reaches a maximum. Total conversion is achieved when $C_++C_-=0$ which implies $\delta\omega=0$, that is only for an incident wave of exact frequency ω_0 . Otherwise, conversion is only partial. Either way however, conversion is directional due to the loss of time-reversal symmetry. Finally, it is desirable to maximize the conversion speed

$$\delta q_d = \frac{\left|1/c_0 - 1/c_j\right|}{2} \sqrt{\delta \omega_{\text{max}}^2 + \delta \omega^2}.$$
 (9)

Variations of δq_d as a function of ω_j are identical to those of $\Im(\delta q)$ plotted on Fig. 4 for a given input mode (q_0,ω_0) and for $\delta\omega=0$ up to exchanging q_j with $-q_j$ since admissible output modes now satisfy $q_0q_j>0$. The conversion distance then turns out to be of the order of $5\pi/Q$.

Numerically simulated transient responses confirm the described non-reciprocal behavior of the modulated metabeam. Let ω_0^A and ω_1^A be, respectively, the lower and higher frequencies of the pair of eigenmodes A and similarly define $\omega_{0,1}^B$. A wave of frequency ω_1^A incident to the left is transmitted unaltered (Fig. 5(a), (b)) but is reflected into a wave of frequency ω_0^A if incident to the right (Fig. 5(c), (d)). As for pair B, a wave of frequency ω_0^B incident to the left is transmitted unaltered (Fig. 6(a), (b)) but is converted into a wave of frequency ω_1^B if incident to the right (Fig. 6(c), (d)). Thus, at ω_0^B , both signals are transmitted but only one experiences a frequency shift. Also on Figs. 5(d) and 6(d), one can observe that in addition to the input and output frequencies $\omega_{0,1}^{A,B}$, there are other frequencies $\omega = \omega_{0,1}^{A,B} \pm \omega_m$ present in the spectrum. These secondary harmonic generation effects are not predicted by the present leading order theory and their modeling requires including higher-order terms in our ansatz.

Mode conversion in the modulated metabeam is not restricted to acoustic–acoustic or optical–optical conversion and the modulation parameters (q_m, ω_m) can be chosen to shift an optical mode (q_0, ω_0) into an acoustic one (q_j, ω_j) as illustrated on Fig. 7. Note that the incident optical mode is such that u and v are completely out of phase whereas the output acoustic mode has u and v in phase. Further, the output frequency being relatively close to the resonance frequency, the signal undergoes a significant amplification.

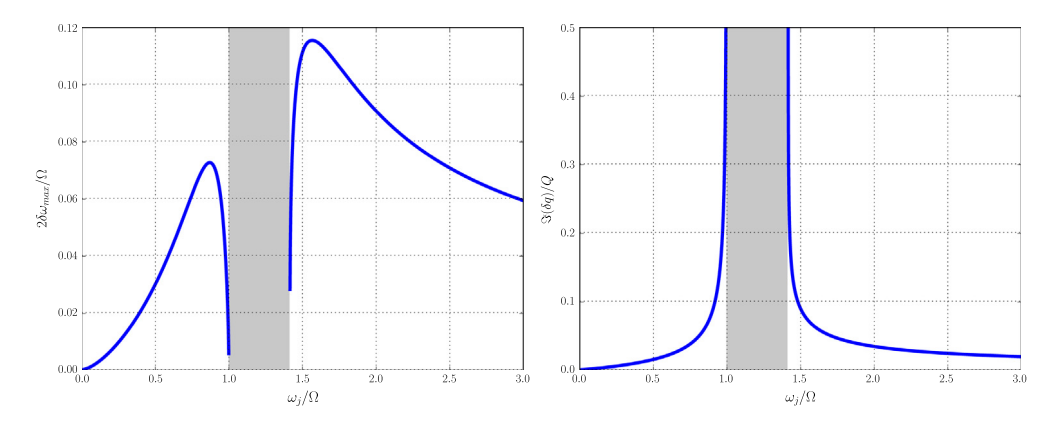


Fig. 4. Variations of $2\delta\omega_{\max}/\Omega$ and $\Im(\delta q)/Q$ as functions of the output frequency ω_l for a given input mode ($q_0=1.046Q$, $w_0=1.664$ Ω); $\delta\omega=0$.

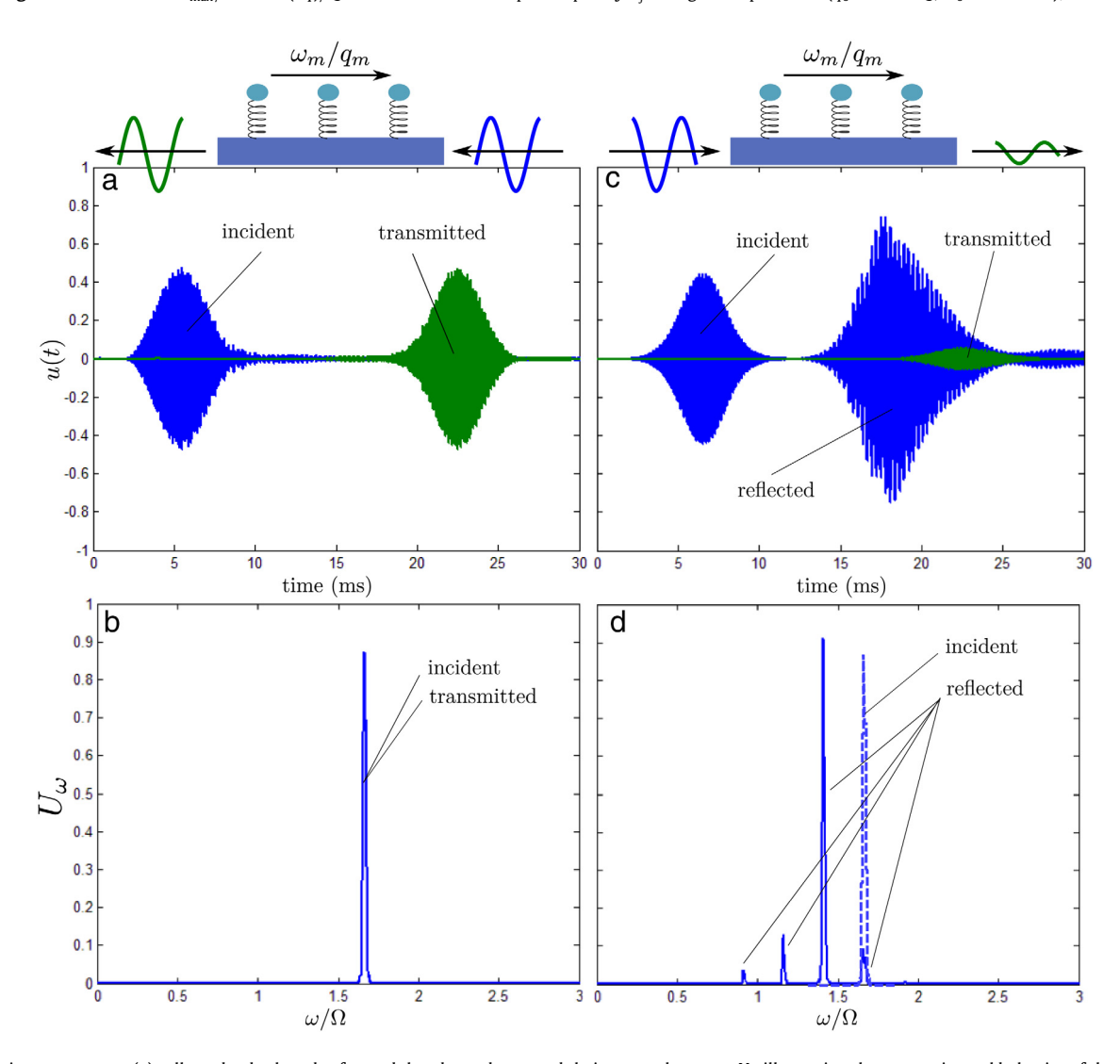


Fig. 5. Transient responses u(t) collected at both ends of a modulated metabeam and their spectral content U_{ω} illustrating the non-reciprocal behavior of the metabeam at $\omega = \omega_1^A$ for a left (a, b) and right (c, d) traveling incident wave. The distance between the input and output locations is about 220/Q.

4. Conclusion

Finally, it is worth mentioning that a remarkable consequence to dispersion is that wave velocity c is no longer uniquely defined. As a result, the usual stability condition [22,23], under which the interactions between the pump and the traveling waves are stable, namely, $|\omega_m/q_m| < c$, does not hold here. It can be deduced from

our results however that stability can still be ensured in the vicinity of a given frequency ω_0 as long as ω_0 is not coupled to any other frequency ω_i such that $\omega_0\omega_i < 0$.

In conclusion, it has been shown that a wide array of non-reciprocal wave phenomena takes place in a modulated medium with strong dispersion effects, both bending- and resonance-generated. These include one-way conversion, transmission and

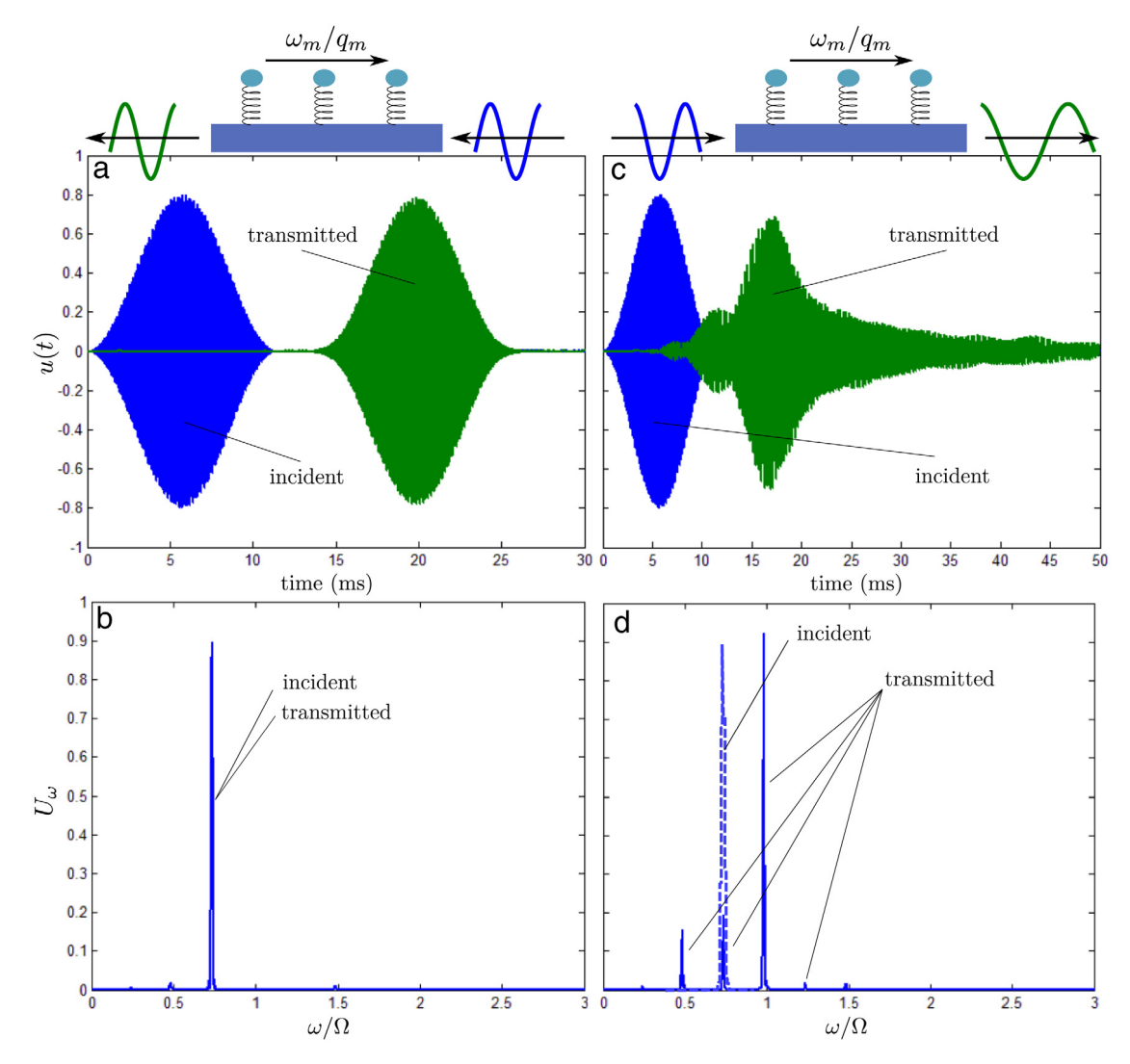


Fig. 6. Transient responses u(t) collected at both ends of a modulated metabeam and their spectral content U_{ω} illustrating the non-reciprocal behavior of the metabeam at $\omega = \omega_0^B$ for a left (a, b) and right (c, d) traveling incident wave. The distance between the input and output locations is about 66/Q.

reflection of waves. It is our hope that the provided analytical quantitative and qualitative results serve as a benchmark for future attempts at designing and carrying experiments to observe the described phenomena.

Acknowledgments

This work is supported by the Air Force Office of Scientific Research under Grant No. AF 9550-15-1-0016 with Program Manager Dr. Byung-Lip (Les) Lee and the NSF EFRI under award No. 1641078.

Appendix A. Directional gap width

In order to prove relation (6), start by expanding the determinant in (5) and solve for δq to find

$$\delta q = \frac{1/c_0 + 1/c_j}{2} \delta \omega$$

$$\pm \sqrt{\frac{\rho'^4 \omega_0^4 \omega_j^4 |\delta_j k|^2}{16q_0^3 q_i^3 G^2 \Pi^2} + \frac{(1/c_0 - 1/c_j)^2}{4} \delta \omega^2}$$
(A.1)

which is imaginary as long as $q_0q_i < 0$ and (6) are satisfied.

Appendix B. Expression of the total field

Eq. (A.1) shows that there are two possible corrections $\delta q_{\pm} = \delta q_s \pm \delta q_d$ for the wavenumber given $\delta \omega$. Accordingly, assuming $q_0 q_j > 0$, the transmitted field has two possible amplitudes U_j^{\pm} given by, say the first line of, (5):

$$U_{j}^{\pm} = -\frac{4q_{0}^{3}G\Pi(\delta q_{\pm} - \delta \omega/c_{0})}{\rho'^{2}\omega_{0}^{2}\omega_{0}^{2}\overline{\delta_{j}k}}U_{0}^{\pm} \equiv C_{\pm}U_{0}^{\pm}.$$
 (B.1)

Hence, the total, incident and transmitted, field admits the expression

$$u(x,t) = \Re \left\{ \left[U_0^+(u_0(x,t) + C_+ u_j(x,t)) e^{i\delta q_d x} + U_0^-(u_0(x,t) + C_- u_j(x,t)) e^{-i\delta q_d x} + \right] e^{i(\delta q_s x - \delta \omega t)} \right\}.$$
(B.2)

Say now that mode u_0 is traveling through a non-modulated metabeam and that, at x=0, it enters into a modulated region. This scenario requires $U_0^+C_+=-U_0^-C_-$ so that there exists a complex number A such that the total field is given by (8).

Appendix C. Finite difference method

Transient responses are simulated using the finite difference method. The governing equations are discretized in space following a centered finite difference scheme with a step of 1 mm; the

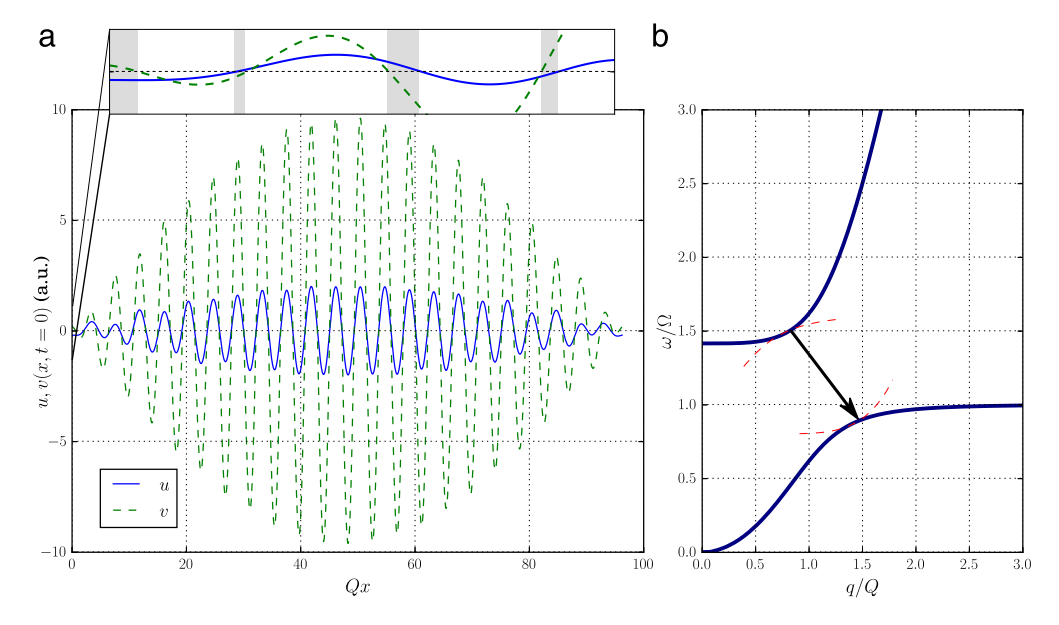


Fig. 7. Variations of u and v as functions of the normalized space variable Qx over twice the conversion distance $\pi/(2\delta q_d)$ (a); zones where u and v are out-of-phase are highlighted in the magnified view. Although initially out-of-phase, at the conversion distance $Qx \approx 50$, u and v become in-phase completing thus an optico-acoustic transition illustrated on (b). Here, the input and output modes are $(q_0 = 0.819Q, \omega_0 = 1.5 \Omega)$ and $(q_j = 1.464Q, \omega_j = 0.89 \Omega)$; the modulation is such that $(q_m = q_0 - q_i = -0.645Q, \omega_m = \omega_0 - \omega_i = 0.61 \Omega)$ and $\delta k/k = 0.1$. Dashed lines on (b) correspond to the translated dispersion curve (see Fig. 2).

beam's total length varied around 1 m. Free boundary conditions were applied. The resulting ordinary differential equations in time are solved with a Runge–Kutta method with a time step of 0.01 ms. The parameters of the metabeam are chosen to facilitate convergence: $Q=223.6~\text{m}^{-1}, \Omega=2.8~\text{kHz}.$

References

- [1] K.A. Lurie, Effective properties of smart elastic laminates and the screening phenomenon, Int. J. Solids Struct. 34 (13) (1997) 1633–1643.
- [2] K.A. Lurie, An Introduction to the Mathematical Theory of Dynamic Materials, Springer, New York, NY, 2007.
- [3] G.W. Milton, O. Mattei, Field patterns: a new mathematical object, Proc. R. Soc. Lond. Ser. A Math. Phys. Eng. Sci. 473 (2017) 20160819.
- [4] E.J. Reed, M. Soljačić, J.D. Joannopoulos, Reversed doppler effect in photonic crystals, Phys. Rev. Lett. 91 (13) (2003) 89–92.
- [5] E.J. Reed, M. Soljačić, M. Ibanescu, J.D. Joannopoulos, Reversed and anomalous Doppler effects in photonic crystals and other time-dependent periodic media, J. Comput. Mater. Des. 12 (1) (2005) 1–15.
- [6] Z. Yu, S. Fan, Complete optical isolation created by indirect interband photonic transitions, Nat. Photonics 3 (2) (2009) 91–94.
- [7] M.B. Zanjani, A.R. Davoyan, A.M. Mahmoud, N. Engheta, J.R. Lukes, One-way phonon isolation in acoustic waveguides, Appl. Phys. Lett. 104 (8) (2014).
- [8] M.B. Zanjani, A.R. Davoyan, N. Engheta, J.R. Lukes, NEMS with broken T symmetry: graphene based unidirectional acoustic transmission lines, Sci. Rep. 5 (2015) 09926.
- [9] N. Swinteck, S. Matsuo, K. Runge, J.O. Vasseur, P. Lucas, P.A. Deymier, Bulk elastic waves with unidirectional backscattering-immune topological states in a time-dependent superlattice, J. Appl. Phys. 118 (6) (2015) 063103.
- [10] G. Trainiti, M. Ruzzene, Non-reciprocal elastic wave propagation in spatiotemporal periodic structures, New J. Phys. 18 (8) (2016) 083047.

- [11] H. Nassar, X.C. Xu, A.N. Norris, G.L. Huang, Modulated phononic crystals: Non-reciprocal wave propagation and Willis materials, J. Mech. Phys. Solids 101 (2017) 10–29.
- [12] J. Gump, I. Finkler, H. Xia, R. Sooryakumar, W.J. Bresser, P. Boolchand, Light-induced giant softening of network glasses observed near the mean-field rigidity transition, Phys. Rev. Lett. 92 (24) (2004) 245501.
- [13] F. Casadei, T. Delpero, A. Bergamini, P. Ermanni, M. Ruzzene, Piezoelectric resonator arrays for tunable acoustic waveguides and metamaterials, J. Appl. Phys. 112 (6) (2012) 064902.
- [14] Y.Y. Chen, R. Zhu, M.V. Barnhart, G.L. Huang, Enhanced flexural wave sensing by adaptive gradient-index metamaterials, Sci. Rep. 6 (2016) 35048.
- [15] Y.Y. Chen, G.L. Huang, C.T. Sun, Band Gap Control in an Active Elastic Metamaterial With Negative Capacitance Piezoelectric Shunting, J. Vib. Acoust. 136 (6) (2014) 061008.
- [16] K. Danas, S.V. Kankanala, N. Triantafyllidis, Experiments and modeling of iron-particle-filled magnetorheological elastomers, J. Mech. Phys. Solids 60 (1) (2012) 120–138.
- [17] F. Li, C. Chong, J. Yang, P.G. Kevrekidis, C. Daraio, Wave transmission in timeand space-variant helicoidal phononic crystals, Phys. Rev. E (3) 90 (5) (2014) 053201.
- [18] R. Chaunsali, F. Li, J. Yang, Stress wave isolation by purely mechanical topological phononic crystals, Sci. Rep. 6 (2016) 30662.
- [19] J.C. Slater, Interaction of waves in crystals, Rev. Modern Phys. 30 (1) (1958) 197–222.
- [20] J.-C. Simon, Action of a progressive disturbance on a guided electromagnetic wave, IRE Trans. Microw. Theory Tech. 8 (1) (1960) 18–29.
- [21] A. Hessel, A.A. Oliner, Wave Propagation in a Medium with a Progressive Sinusoidal Disturbance, IRE Trans. Microw. Theory Tech. 9 (4) (1961) 337–343.
- [22] E.S. Cassedy, A.A. Oliner, Dispersion Relations in Time-Space Periodic Media: Part II-Unstable Interactions, Proc. IEEE 51 (10) (1963) 1342–1359.
- [23] E.S. Cassedy, A.A. Oliner, Dispersion Relations in Time-Space Periodic Media: Part I-Stable Interactions, Proc. IEEE 51 (10) (1963) 1342–1359.
- [24] H. Nassar, H. Chen, A.N. Norris, M.R. Haberman, G.L. Huang, Non-reciprocal wave propagation in modulated elastic metamaterials, Proc. R. Soc. Lond. Ser. A Math. Phys. Eng. Sci. 473 (2017) 20170188.